Research Article

Mohammed Bourhia*, Muhammad Shahab, Guojun Zheng, Mohamed Taibi, Amine Elbouzidi, Ahmad Mohammad Salamatullah, Musaab Dauelbait*, Abdeslam Asehraou

Overcoming methicillin resistance by methicillin-resistant *Staphylococcus aureus*: Computational evaluation of napthyridine and oxadiazoles compounds for potential dual inhibition of PBP-2a and FemA proteins

https://doi.org/10.1515/chem-2024-0082
received April 13, 2024; accepted August 18, 2024

Abstract: The treatment of the various infections caused by *Staphylococcus aureus* has become challenging due to the evolving resistance against current therapeutics. In this study, the potentials of napthyridine and oxadiazole derivatives to serve as dual inhibitors of penicillin-binding protein 2a (PBP-2a) and FemA protein, which are crucial to resistance to methicillin-based drugs by *S. aureus*, were evaluated using molecular modeling techniques. Seventy-two compounds were subjected to molecular docking against the proteins, and the hit compounds were subjected to drug-likeness evaluation and in silico pharmacokinetics prediction. The compounds with good safety profiles were subjected to a 250-ns molecular dynamics (MD) simulation and other relevant analyses based on the MD trajectories. Five hit compounds were selected based on their high affinity for the targets as evidenced by their docking scores ranging from −8.6 to −10.1 kcal/mol for PBP-2a and −9.6 to −9.9 kcal/mol for FemA. These compounds also passed Lipinski's rule of five evaluation with no violation and possessed high human intestinal absorption potential, showcasing their potential as orally administered therapeutic agents. However, three of the compounds were potential mutagens. MD simulation revealed that the final two compounds maintained stable interactions with the target proteins over 250 ns, with minimal deviations and fluctuations. Hydrogen bond stability and energy decomposition analysis further confirmed the strong binding affinity of the hit compounds compared to the control drug, methicillin. Conclusively, the compounds with the CID "135964525" and "44130718" are worthy of further experimental validation in the development of potential inhibitors of PBP-2a and FemA.

Keywords: methicillin-resistance, *Staphylococcus aureus*, napthyridine compound, oxadiazoles compound, PBP-2a protein, FemA protein

*** Corresponding author: Mohammed Bourhia**, Department of Chemistry and Biochemistry, Faculty of Medicine and Pharmacy, Ibn Zohr University, Laayoune, 70000, Morocco, e-mail: m.bourhia@uiz.ac.ma
*** Corresponding author: Musaab Dauelbait**, Department of Scientific Translation, Faculty of Translation, University of Bahri, Khartoum, 11111, Sudan, e-mail: musaabelnaim@gmail.com
Muhammad Shahab, Guojun Zheng: State Key Laboratories of Chemical Resources Engineering, Beijing University of Chemical Technology, Beijing, 100029, PR China
Mohamed Taibi, Amine Elbouzidi: Laboratoire d'Amélioration des Productions Agricoles, Biotechnologie et Environnement (LAPABE), Faculté des Sciences, Université Mohammed Premier, Oujda, 60000, Morocco
Ahmad Mohammad Salamatullah: Department of Food Science & Nutrition, College of Food and Agricultural Sciences, King Saud University, 11 P.O. Box 2460, Riyadh, 11451, Saudi Arabia
Abdeslam Asehraou: Laboratory of Bioresources, Biotechnology, Ethnopharmacology and Health, Faculty of Sciences, Mo-hammed First University, Boulevard Mohamed VI, B.P. 717, Oujda, 60000, Morocco

1 Introduction

Staphylococcus aureus, commonly known as *S. aureus*, is a versatile and medically significant bacterial species that continues to be a formidable public health threat worldwide [1]. First identified in the late 19th century by Sir Alexander Ogston, *S. aureus* quickly gained notoriety as a leading causative agent of various infectious diseases [2]. Its ability to colonize and infect a wide range of host tissues and evade the human immune response has rendered it a cynosure in scientific research. Initially, *S. aureus* was primarily associated with skin and soft tissue infections; however, it has now expanded its repertoire to include more

invasive and life-threatening diseases, such as bacteremia, endocarditis, osteomyelitis, and necrotizing pneumonia [3]. *S. aureus* is a highly contagious bacterium that can spread via direct or indirect contact with infected people or contaminated surfaces. The most common mode of transmission is through skin-to-skin contact, particularly in crowded settings such as hospitals, schools, and athletic facilities [4]. *S. aureus* can also be transmitted through contact with infected wounds, sores, or lesions on the skin, a mode of transmission that is mostly prevalent in healthcare settings, where patients with open wounds or surgical incisions are at elevated risk of infection [5].

The treatment of infections caused by *S. aureus* presents significant challenges, particularly because of the rise of antibiotic-resistant strains like methicillin-resistant *Staphylococcus aureus* (MRSA) [6]. A notable strategy employed in the treatment of *S. aureus* infection involves a combination of antimicrobial therapies due to the reduced efficacy of monotherapies [7]. In resistant strains such as MRSA, certain cellular proteins are responsible for the development of resistance to antimicrobials, exemplifying this is the penicillin-binding protein 2a (PBP-2a). PBP-2a is a crucial enzyme in MRSA, responsible for cell wall biosynthesis, and it plays a key role in MRSA's resistance to β-lactam antibiotics [8]. Generally, β-lactam antibiotics mediate deleterious actions on *S. aureus* by inhibiting the production of peptidoglycan in reactions catalyzed by penicillin-binding proteins (PBPs) [9]. The peptidoglycan is an essential component of the bacterial cell wall, and its inhibition leads to cell lysis and bacterial death. However, MRSA, through the action of PBP-2a, has developed a mechanism to resist the effects of β-lactam antibiotics [8]. The PBP-2a proceeds to mediate the transpeptidase reaction required for peptidoglycan biosynthesis, even in the presence of β-lactam drugs [10], contributing significantly to MRSA's ability to endure and multiply even when β-lactam antibiotics are present, ultimately rendering the traditional treatment ineffective. Similarly, the FemA protein, encoded by the Fem genes, is a cytoplasmic protein which is crucial for the expression of methicillin resistance in MRSA. It has been reported to mediate the expression of the mecA gene, which encodes the PBP-2a protein, intriguingly, the absence of FemA conferred susceptibility to methicillin [11,12]. As a result, inhibiting these proteins has become a promising strategy for fighting *S. aureus* infections.

Napthyridine and oxadiazoles derivatives have garnered attention in medicinal chemistry research for their potential to combat microbial infections and other diseases. Specifically, napthyridine derivatives have shown pharmacological effects, such as antiviral, anticancer, anti-inflammatory, antimalarial, and antiprotozoal, among various other properties [13,14,15]. Similarly, oxidiazole derivatives have shown a broad spectrum of pharmacological properties, including antioxidant, anthelmintic, anti-inflammatory, cytotoxic, and anticonvulsant activities [16], with some reported to also possess antitubercular, anti-HIV, anti-hypertensive, and anticancer properties [17]. Consequently, both napthyridine and oxadiazole derivatives are explored in drug discovery studies against a wide range of infections.

This study aims to evaluate the potentials of the derivatives of napthyridine and oxadiazoles derivatives as inhibitors of the PBP-2a of *S. aureus* using computer-aided drug design (CADD) including virtual screening, drug-likeness evaluation, and pharmacokinetics properties profiling, quantum mechanical calculations, and molecular dynamics (MD) simulation. It is worth noting that CADD has shifted the paradigm in drug discovery by improving the cost- and time-effectiveness of this process [18].

2 Methods

2.1 Ligand retrieval and preparation

Oxadiazoles and napthyridine derivatives were identified by searching the PubChem database (https://pubchem.ncbi.nlm.nih.gov/). The keywords "napthyridine" and "oxadiazoles" were used to identify the respective napthyridine and oxadiazole derivatives available on the PubChem database. The identified derivative structures were obtained in structure data format [19,20] and were imported into PyRx via the incorporated OpenBabel module. Subsequently, the structures were subjected to energy minimization using the universal forcefield and the conjugate gradients algorithm [21].

2.2 Target structure retrieval and preparation

The three-dimensional (3D) structure of PBP-2a was elucidated using the X-ray diffraction method obtained from the Protein Databank (PDB) (https://www.rcsb.org/) [22] in PDB format using the PDB ID: 5M18 [23]. Also, the 3D structure of FemA was retrieved with the PDB ID: 1LRZ [24]. Sequel to the retrieval of the structure, it was prepared using the Dock prep module of UCSF Chimera v1.10.2 software program [25]. The preparation steps involved removing heteroatoms, water molecules, and associated ligands while restoring missing hydrogen atoms and charge ions. Subsequently, the Dock-prepped structure was subjected to energy minimization procedures using the energy minimization algorithm of

the Swiss-PdbViewer v.4.10 software program [19,26]. Noteworthy, the energy minimization of the protein structure was done in vacuo using the GROMOS 43B1 forcefield which allows the evaluation of the energy of a structure as well as the repairing of distorted geometries [26].

2.3 Molecular docking simulation

A flexible docking protocol was employed to study the interaction of the compounds with the PBP-2a using the VINA module incorporated into the Python Prescription suite v.0.8 [27]. For the PBP-2a, the amino acid residues that constitute the active site of the protein were firstly delineated using the BIOVIA Discovery studio visualizer, after which a grid box of size x = 17.1656237844 Å, y = 22.4011654882 Å, and z = 12.9173766199 Å, with a center dimension of x = 17.4802893733, y = −18.9999491012, and z = −50.2219055 were set to define the active site. Conversely, a blind docking protocol was employed to study the interactions of the compounds with FemA, the grid box with size x = 68.8990970136 Å, y = 85.8606218435 Å, and z = 52.064913585 Å, with a center dimension of x = 35.0115192852, y = 68.8214808942, and z = 94.3147800551 was found to cover every residue of the protein. The docking procedure was initially executed using the default exhaustiveness of "8," and finally, using the highest exhaustiveness of "32" which is available for AutoDock Vina. Following the docking simulation, the interactions of the protein with the ligands were studied using BIOVIA Discovery Studio [28].

2.4 Druglikeness and pharmacokinetics properties profiling

The Simplified Molecular Input Line Entry System (SMILES) of the hit compounds identified after the docking simulation were retrieved from the PubChem database and utilized for evaluating the drug-likeness of the compounds in accordance with Lipinski's rule of five (Ro5) [29]. The SwissADME webserver (https://www.swissadme.ch.index.php/) was employed for this purpose [30], while the pharmacokinetics and toxicity profiles of the compounds were assessed using the pkCSM server (https://biosig.lab.uq.edu.au/pkcsm/prediction) [31].

2.5 MD simulation of top-scoring hits

The top-scoring viable hits for each of the protein and control drugs were subjected to MD simulation and free energy calculation-based validation was performed using AMBER v.22 (Case et al. [32]; Pearlman et al. [33]). The TIP3P water model was used, and the system was neutralized by Na^+ counter ions addition (Wang et al. [34]). The General Amber Force Field-2 (GAFF2) was used to parameterize the small selected molecules [35] with the estimation of AM1-BCC charges [35]. The steepest descent algorithm was used to minimize the energy of the system. Prior to the simulations, a restricting simulation of position for equilibration around both system and solvent with protein was carried out. MD simulation studies of the system were performed using NPT and NVT ensembles with a fixed number of atoms, volume, pressure, and temperature. Hydrogen bonds were constrained by the Particle Mesh Ewald SHAKE algorithm. Finally, 200 ns MD simulation was performed for each system. The MD trajectories were analyzed by root mean square deviation (RMSD), root mean square fluctuation (RMSF), etc., using CPPTRAJ and PYTRAJ. Visualization was performed with PyMol [36]. Furthermore, we also calculated the total energies of all the systems, including control and final hits.

2.5.1 Binding free energy calculations

We computed the binding free energy of WT-MT complexes using the MMGBSA method [37]. The calculation was performed on 20,000 conformations collected after each 0.2 ns in the course of all-atom (200 ns) trajectories. Two widely used methods to calculate the free energy are mechanics Poisson–Boltzmann surface area (MM/PBSA) and molecular mechanics/generalized Born surface area (MM/GBSA). Experimental approaches are corroborated by the values of MM/PBSA [38]. In protein–protein interaction and protein-ligand binding, MM/PBSA has been widely used. In our case, we run each using the MMPBSA and MMGBSA approach to calculate the binding free energy.

The following equation was used for free energy calculation:

$$\Delta G(\text{bind}) = \Delta G(\text{complex}) - [\Delta G(\text{receptor}) + \Delta G(\text{ligand})],$$

$$G = G_{\text{bond}} + G_{\text{ele}} + G_{\text{vdW}} + G_{\text{pol}} + G_{\text{npol}} - \text{TS}.$$

Here, G_{bond}, G_{ele}, and G_{vdW} refer to bonded, electrostatic, and van der Waals (vdW) interactions, respectively. G_{pol} and G_{npol} are polar and nonpolar solvated free energies. The G_{pol} and G_{npol} are calculated by the generalized Born (GB) implicit solvent method with the solvent-accessible surface area (SASA) term. We additionally carried out per-residues energy decomposition analysis to identify which residue contributes how much of the total interaction (energy).

3 Results and discussion

3.1 Retrieved ligands and target structures

A thorough search of the PubChem database revealed 12 oxadiazoles and 65 naphthyridine derivatives of which the oxadiazoles were majorly the 1,3,4-oxadiazole while the naphthyridine derivatives included the 1,5-napthyridine, 1,6-napthyridine, 1,7-napthyridine, and 1,8-napthyridine derivatives. The structure of PBP-2a with a resolution of 1.98 Å was retrieved in a complex with cefepime ligand, structural analysis revealed the protein to be a homodimer composed of 642 amino acid residues. Conversely, the retrieved FemA structure has a resolution of 2.1 Å, was not in complex with an inhibitor, and is composed of 426 amino acid residues. The retrieved structures of the protein are depicted in Figure S1. In preparation for molecular docking, the chain A of the PBP-2a was selected and prepared, while structures of FemA and the ligands were also prepared.

3.2 Molecular docking simulation

The docking simulation results revealed the exhaustiveness parameter greatly affects the docking scores of the compounds for the proteins, with the "32" exhaustiveness value correlating to lower docking scores on most occasions. As presented in the Supplementary material, the compounds with the CIDs "9965471," "89995619," "85199," and "66997784" had initial docking scores of −6.8, −5.9, −6.0, and −9.2 kcal/mol, respectively, against FemA when the exhaustiveness parameter value was "8," interestingly, the docking scores further increased to −6.6, −5.3, −5.7, and −7.9 kcal/mol, respectively, when the exhaustiveness parameter was set to "32," indicating the elimination of false positives. Similarly, the compounds with the CIDs "10129935," "10523409," "10546084," and "10571743" had initial docking scores of −3.9, −8.5, −7.7, and −8.4 kcal/mol, respectively, against PBP-2a, while the final docking scores were −3.9, −8.0, −7.5, and −8.4 kcal/mol. Consequently, the hit compounds of this study were selected based on the docking scores obtained with the exhaustiveness set to "32," and the selected compounds are presented in Table 1. As evident in the table, the selected compounds possessed higher affinities for the proteins compared to methicillin.

3.3 Molecular interaction profiling

The interactions of the hit compounds of this study with PBP-2a and FemA are depicted in Figures 1 and 2, respectively. The compounds interacted with multiple amino acid residues in the binding site of the proteins, with many interactions including vdW interactions, hydrogen bonds, pi-sigma, and pi-sulfur bonds present.

Table 1: The docking scores of the hit compounds against PBP-2a and FemA proteins

S/N	Compound CID	Docking scores (kcal/mol)	
		PBP-2a	FemA
1	135964525	−10.1	−9.8
2	44130718	−9.5	−9.9
3	135438537	−9.1	−9.4
4	135505656	−9.1	−9.4
5	135520508	−8.6	−9.6
6	Methicillin	−6.4	−6.6

3.4 Drug-likeness assessment and pharmacokinetics profiling

The drug-likeness of the hit compounds of this study was assessed based on the Ro5 to determine their viability to serve as orally active drugs in humans. As evident in Table 2, none of the hit compounds of this study violated the Ro5; hence, they are all drug-like.

The ADMET properties of the hit compounds are also presented in Table 3. All the compounds possessed higher intestinal absorption potentials compared to methicillin; however, they all possess the potential to inhibit P-glycoprotein I and II (Table 3). Disappointingly, three of the compounds which are "135438537," "135505656," and "135520508" were predicted to be AMES toxic.

3.5 All atoms MD simulation of the final complexes

As evident in Figure 3, the complexes formed by the individual compound with the best docking scores for FemA and PBP-2a, as well as the complexes formed by the standard drug (methicillin) were selected for MD simulation, the complexes are PBP-2a_Methicillin and PBP-2a_44130718, and FemA_methicillin and FemA_135964525 complexes.

3.5.1 Dynamic stability assessment analysis

The RMSD of the FemA apoprotein (FemA_Apo), FemA_methicillin, and FemA_135964525 during the 250 ns simulation period

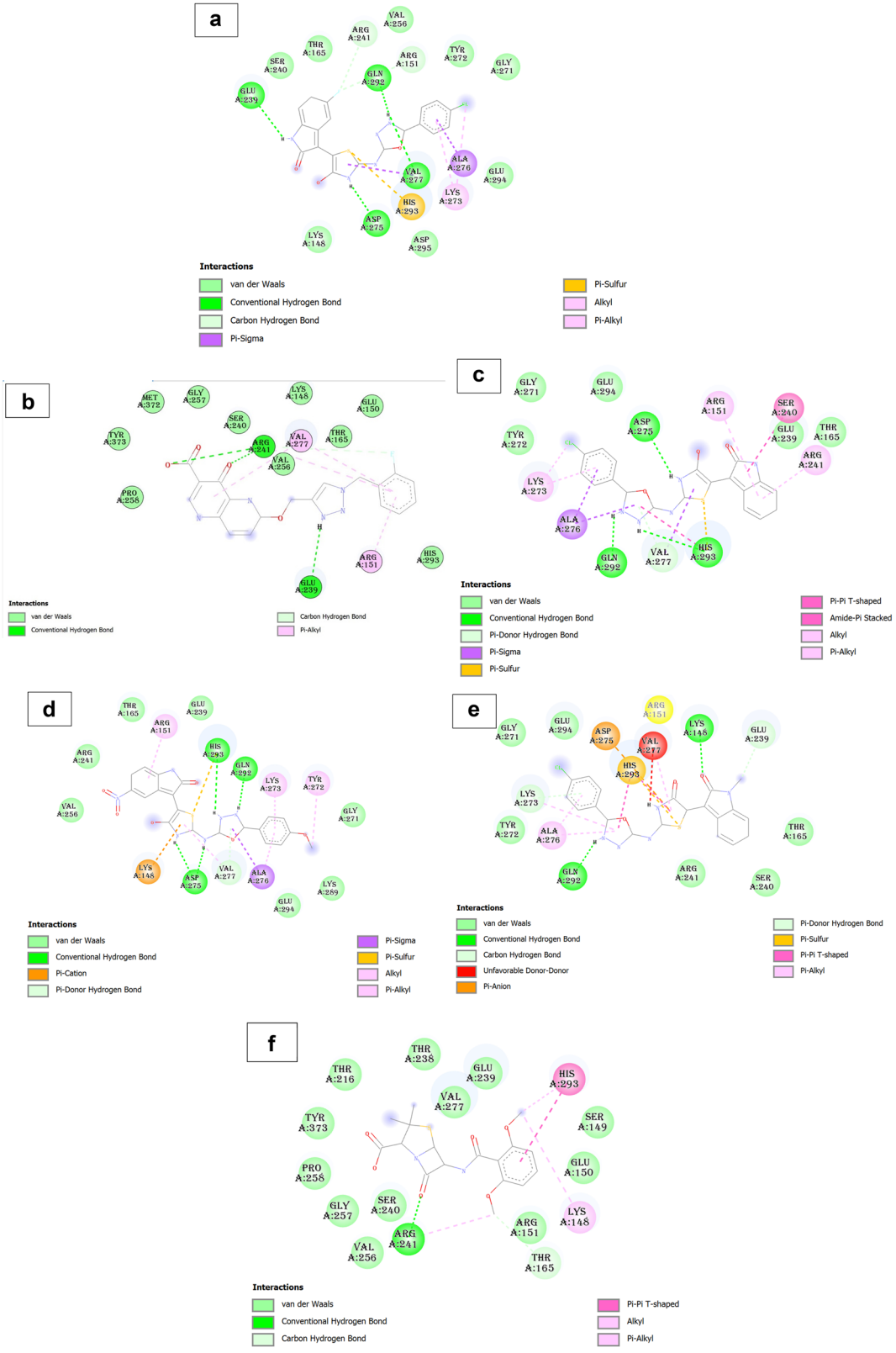

Figure 1: The interaction of the hit compounds of this study with PBP-2a protein. (a) PBP2a-44130718; (b) PBP2a-44130718; (c) PBP2a-135505656; (d) PBP2a-135520508; (e) PBP2a-135964525; and (f) PBP2a-Methicillin.

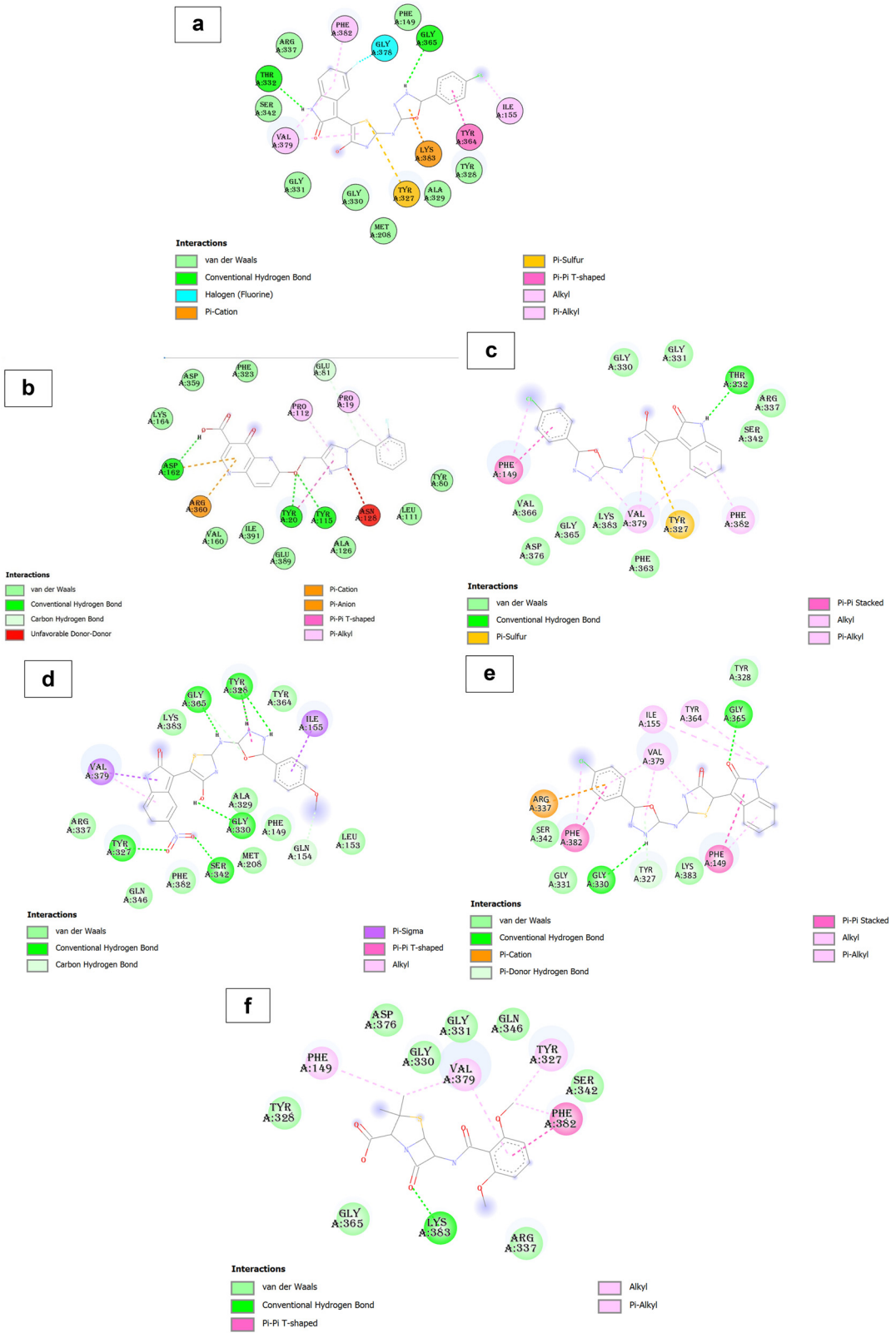

Figure 2: The interaction of the hit compounds of this study with FemA protein. (a) FemA-44130718; (b) FemA-44130718; (c) FemA-135505656; (d) FemA-135520508; (e) FemA-135964525; and (f) FemA-methicillin.

Table 2: The physicochemical properties of the hit compounds based on the Ro5

Compound	MW (Da)	NHBA	NHBD	MLOGP	Violations
135964525	437.86	6	1	3.21	0
44130718	395.34	6	0	3.53	0
135438537	437.40	9	2	2.96	0
135505656	423.83	7	2	3.22	0
135520508	464.41	10	2	1.93	0
Methicillin	380.42	6	2	1.06	0

are depicted in Figure 3a, while that of PBP-2a apoprotein (PBP-2a_Apo), PBP-2a_methicillin, and PBP-2a_44130718 are presented in Figure 3b.

3.5.2 Protein residual flexibility analysis

The RMSF of the FemA apoprotein (FemA_Apo), FemA_methicillin, and FemA_135964525 during the 250 ns simulation period are depicted in Figure 4a, while that of PBP-2a apoprotein (PBP-2a_Apo), PBP-2a_methicillin, and PBP-2a_44130718 are presented in Figure 4b.

3.5.3 Assessment of structural packing and residue flexibility

The radius of gyration, or structural packing, is a key metric for assessing protein size variation throughout the simulation time. It also provides crucial insights into the stability of the protein. Furthermore, this method has been significantly used to detect the binding and unbinding events throughout the simulation. The radius of gyration plots for the complexes are depicted in Figure 5(a) and (b).

3.5.4 Hydrogen bonding analysis

The persistence of the hydrogen bond over 250 ns simulation was plotted and is depicted in Figure 6.

3.5.5 Per-residues energy decomposition analysis

To assess the impact of each residue and its contribution to the total binding energy, a per-residue energy decomposition analysis was performed on the trajectory file obtained

Table 3: The drug-likeness profile and pharmacokinetics properties of the hit compounds of this study

Models	Compounds					
	135964525	44130718	135438537	135505656	135520508	Methicillin
Absorption						
HIA	100	57.839	93.029	93.827	86.196	45.343
Water solubility	−4.278	−2.992	0.583	0.679	−3.352	−2.628
Caco-2 permeability	1.023	0.993	−3.236	−3.143	0.45	0.563
P-gp (substrate)	Non-substrate	Substrate	Substrate	Substrate	Substrate	Substrate
P-gp I (inhibitor)	Inhibitor	Non-inhibitor	Inhibitor	Inhibitor	Inhibitor	Non-inhibitor
P-gp II (inhibitor)	Inhibitor	Non-inhibitor	Inhibitor	Inhibitor	Inhibitor	Non-inhibitor
Distribution						
Fraction unbound	0	0.245	0	0	0.022	−1.62
Metabolism						
CYP450 2C9 (inhibition)	Inhibitor	Non-inhibitor	Non-inhibitor	Inhibitor	Inhibitor	Non-inhibitor
CYP450 2D6 (substrate)	Non-substrate	Non-substrate	Non-substrate	Non-substrate	Non-substrate	Non-substrate
CYP450 2D6 (inhibition)	Non-inhibitor	Non-inhibitor	Non-inhibitor	Non-inhibitor	Non-inhibitor	Non-inhibitor
CYP450 3A4 (substrate)	Substrate	Non-substrate	Substrate	Non-substrate	Substrate	Non-substrate
CYP450 3A4 (inhibition)	Inhibitor	Non-inhibitor	Inhibitor	Non-inhibitor	Inhibitor	Non-inhibitor
CYP450 1A2 (inhibition)	Non-Inhibitor	Non-inhibitor	Non-Inhibitor	Inhibitor	Non-Inhibitor	Non-Inhibitor
CYP450 2C19 (inhibition)	Inhibitor	Non-inhibitor	Inhibitor	Non-inhibitor	Non-inhibitor	Non-inhibitor
Excretion						
Renal organic cation transporter 2 (OCT2)	Non-substrate	Non-substrate	Non-substrate	Non-substrate	Non-substrate	Non-substrate
Toxicity						
AMES toxicity	Non-toxic	Non-toxic	Toxic	Toxic	Toxic	Non-toxic
hERG I inhibitor	Non-inhibitor	Non-inhibitor	Non-inhibitor	Non-inhibitor	Inhibitor	Non-inhibitor
Skin sensitization	No	No	No	No	No	No

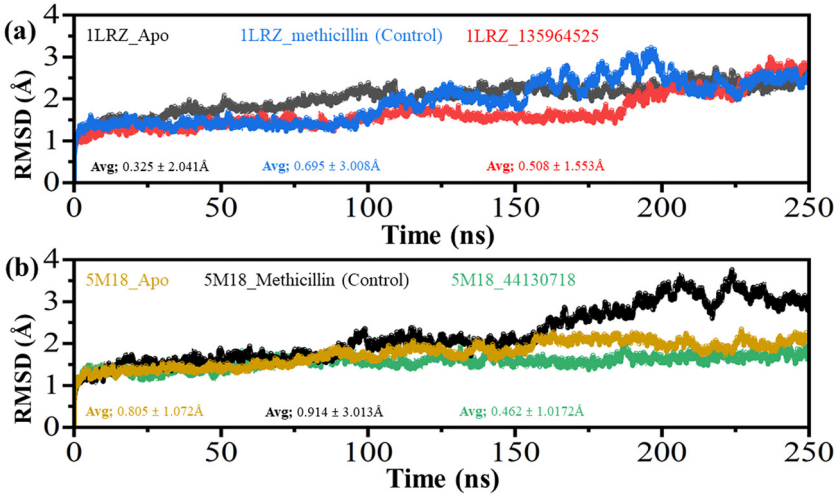

Figure 3: RMSD analysis of FemA complexes over a 250 ns simulation period. (a) The RMSD graph of FemA_Apo, FemA_methicillin, and FemA_135964525 complexes. (b) The RMSD of PBP-2a_Apo, PBP-2a_Methicillin (control), and PBP-2a_44130718 complexes.

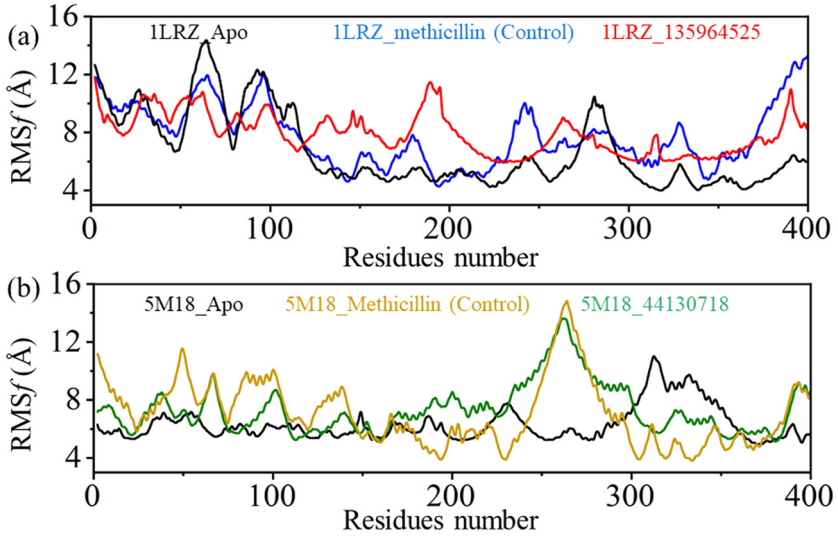

Figure 4: Residual flexibility result of final complexes. (a) The RMSF results for the FemA_Apo, FemA_methicillin (control) and FemA_135964525 (b) PBP-2a_Apo, PBP-2a_Methicillin (control) and PBP-2a_44130718.

from the 250 ns simulation and the results are depicted in Figure 7.

3.5.6 Binding free energy calculations

Free energy computation and analysis were conducted to quantitatively compare the interaction changes between the control drug and the designed drug systems. A total of 5,000 snapshots from the last 250 ns of the MD simulation trajectory were used to calculate the total free energy. Each contributing term, including vdW, electrostatic, polar solvation, and SASA energies, was calculated and is presented in Table 4 (MM/GBSA). The MM/GBSA results also show variations in energies between the control drug and the hit compounds, with the most significant differences observed in total and electrostatic energies.

4 Discussion

Globally, the treatment of *S. aureus* has become challenging due to the emergence of resistant strains; hence, the search for alternative drugs that can be used in its treatment is ongoing. In this study, 72 compounds were

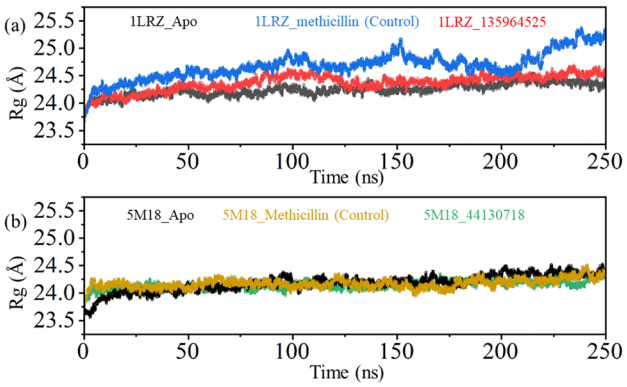

Figure 5: Radius of gyration result of final complexes. (a) The Rg results for the FemA_Apo, FemA_methicillin (control) and FemA_135964525 and (b) PBP-2a_Apo, PBP-2a_Methicillin (control) and PBP-2a_44130718.

virtually screened to evaluate their potential as inhibitors of two crucial MRSA proteins.

A semi-flexible docking methodology revealed that the selected hit compounds exhibited high affinity for the targets, with docking scores ranging from −8.6 to −10.1 kcal/mol for PBP-2a and from −9.6 to −9.9 kcal/mol for FemA. In this study, we applied two different exhaustiveness values, "8" and "32." The exhaustiveness parameter in AutoDock Vina controls the depth and thoroughness of the conformational search for optimal ligand binding poses. The default exhaustiveness value in AutoDock Vina is "8," and it provides a balance between computational efficiency and search thoroughness. This setting allowed us to perform initial screenings rapidly while maintaining reasonable accuracy in identifying potential binding poses. However, increasing the exhaustiveness to 32 significantly enhanced the thoroughness of the conformational search. Although this higher setting required more computational resources and time, it resulted in a more detailed exploration of the ligand binding space, hence, improving the reliability of our docking results and enabling a more precise identification of the best binding poses and interactions. Interestingly, a study by Agarwal and Smith, in which they evaluated the effect of box sizes and exhaustiveness values on AutoDock Vina-generated ligand pose accuracy, reported that utilizing the default exhaustiveness value will likely lead to the generation of false positive results, while values greater than 25 have minimal contribution to the quality of the results at the expense of computational time [39]. Hence, it can be concluded that the value utilized in this study gives the best results that can be obtained using AutoDock Vina.

The hit compounds of this study interacted with relevant amino acid residues of PBP-2a. The compound with the CID "135964525" formed hydrogen bonds with LYS148 and GLN292, and formed Van der Waals interactions with THR165, SER240, ARG241, GLY271, TYR272, and GLU294. It

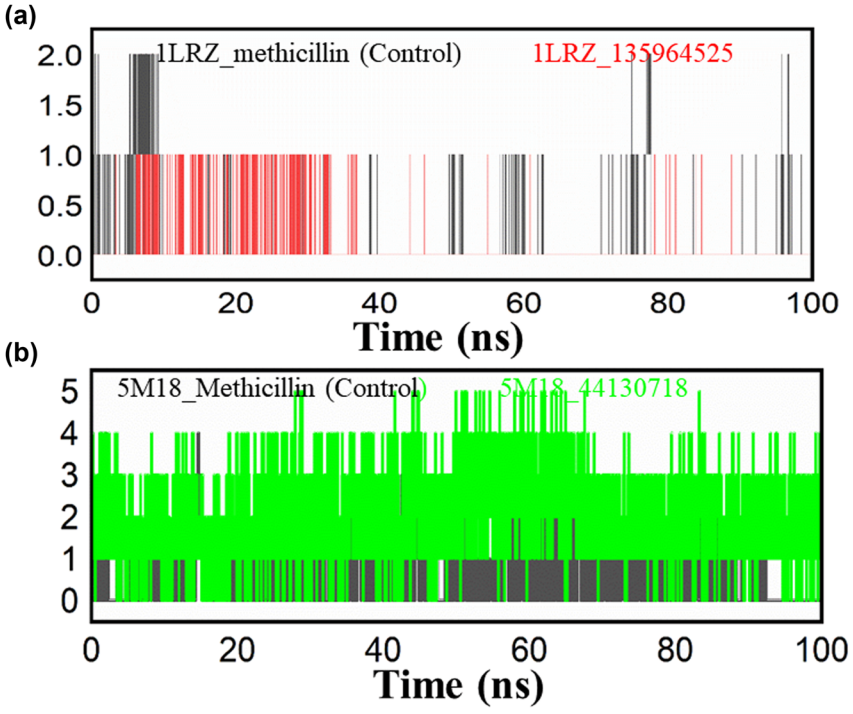

Figure 6: The persistence of the hydrogen bond over 250 ns simulation was plotted and is depicted in Figures 6a and b.

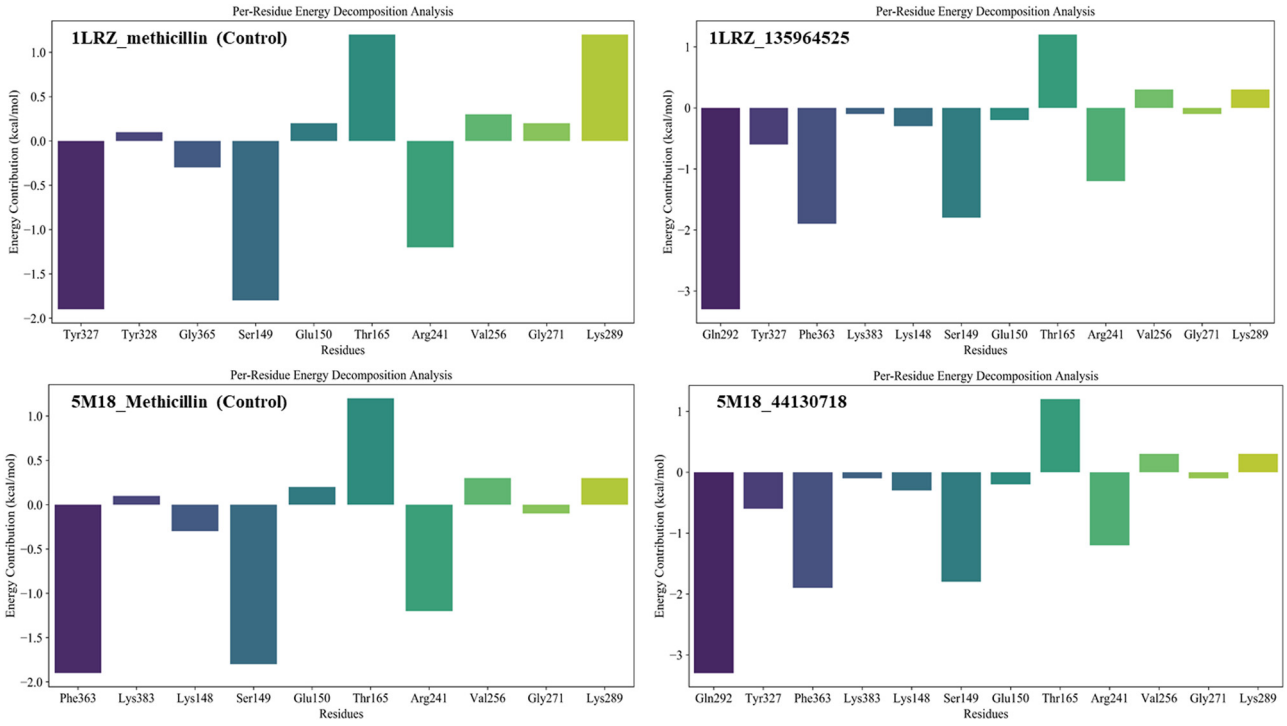

Figure 7: The figure showing energy per-residue energy decomposition analysis contributing to the total energy. All the energies are given in kcal/mol.

also formed pi-sulfur interaction with HIS293, pi-donor interactions with GLU239 and LYS273, pi-anion interaction with ASP275, and pi-alkyl interaction with ALA276. Similarly, compound "44130718" formed two hydrogen bonds with GLU239 and ARG241, vdW interaction with LYS148, GLU150, THR165, SER240, VAL256, GLY257, PRO258, HIS293, MET372, and TYR373, formed pi-alkyl with ARG151 and VAL277. Compound "135425237" formed hydrogen bond with GLU239, ASP275, and VAL277; pi-sulfur interaction with HIS293; pi-sigma interaction with ALA276; vdW interaction with LYS148, THR165, SER240, VAL256, GLY271, TYR272, GLU294, and ASP295; and carbon hydrogen bond with ARG151 and ARG241. Compound "135505656" formed hydrogen bond with ASP275, GLN292, and HIS293; vdW interaction THR165, GLU239, GLY271, TYR272, and GLU294; pi-donor interaction with VAL277; pi-sigma interaction with ALA276; and pi-alkyl interaction with ARG151, ARG241, and LYS273. Compound "135520508" formed two hydrogen bonds with ASP275 and one hydrogen bond with GLN292 and HIS293; vdW interaction with THR165, GLU239, ARG241, VAL256, GLY271, LYS289, and GLU294; pi-cation interaction with LYS148; pi-donor interaction with VAL277; pi-sigma interaction with ALA276; and pi-alkyl interactions with ARG151, TYR272, and LYS273. The standard drug (methicillin) formed hydrogen bonds with LYS148 and GLN292; vdW interactions with SER149, GLU150, ARG151, THR216, THR238, GLU239, SER240, VAL256, GLY257, PRO258, VAL277, and TYR373; carbon–hydrogen bond with THR165; pi–pi T-shaped with HIS293; and pi–pi alkyl interaction with LYS148. It is worth noting that the interactions of these compounds are with the allosteric site residues of PBP-2a, which control the activity of the active site of the protein [23], and the residues with which they interacted were similar to those reported by Aribisala and Sabiu for their hit compounds [40].

Table 4: MM/PBSA of wild-type and mutant systems

Complex name	MMPBSA (kJ/mol)			
	Δ_{vdW}	Δ_{elec}	Δ_{ps}	$\Delta_{G,total}$
1LRZ_methicillin	−31.28 ± 12.66	−1317.27 ± 94.28	1227.43 ± 169.48	−35.41 ± 35.11
1LRZ_135964525	−53.88 ± 11.13	−1501.34 ± 100.01	1691.063 ± 109.13	−42.54 ± 12.30
5M18_Methicillin	−42.58 ± 16.14	−1103.16 ± 101.35	1180.23 ± 98.691	−31.01 ± 12.21
5M18_44130718	−53.56 ± 11.63	−1501.61 ± 131.16	1512.22 ± 83.58	−35.41 ± 11.20

The interaction of the hit compounds with FemA also included hydrogen bond interactions among others. The compound "135425237" interacted with FemA via hydrogen bond with THR332 and GLY365; vdW interactions with PHE149, MET208, TYR328, ALA329, GLY330, GLY331, ARG337, and SER342; pi-sulfur interactions with TYR327; pi-cation interaction with LYS383; halogen-based interaction with GLY378; and alkyl and pi-alkyl interactions with ILE165, VAL379, and PHE382. Compound "44130718" formed hydrogen bonds with TYR20, TYR115, and ASP162; carbon–hydrogen bond with GLU81; vdW interactions TYR80, LEU111, ALA126, VAL160, LYS164, PHE323, ASP359, GLU389, and ILE391; pi-donor interactions with ARG36 and ASP162; pi-alkyl interaction with PRO19 and PRO112; pi–pi T-shaped interaction with TYR20; and an unfavorable donor–donor interaction with ASN128. Compound "135505656" formed just one hydrogen bond with THR332; vdW interactions with GLY330, GLY331, ARG337, SER342, PHE363, GLY365, VAL366, ASP376, and LYS383; pi-sulfur interaction with TYR327; pi–pi stacked interaction with PHE149; two pi-alkyl interactions with VAL379 and another with PHE382; and an alkyl interaction with VAL379. Compound "135520508" formed hydrogen bonds with TYR327, GLY330, SER342, GLY365 and two hydrogen bond interactions with TYR328; vdW interactions with PHE149, LEU153, MET208, ALA329, ARG337, GLN346, TYR364, and PHE382; pi-sigma interactions with ILE155 and VAL379; and pi–pi T-shaped interaction with TYR328. Compound "135964525" interacted with GLY330 and GLY365; vdW interactions with TYR328, GLY331, SER342, LYS383; pi-donor hydrogen bond with TYR327; pi–pi stacked interactions with PHE149 and PHE382; pi-alkyl interactions with PHE149 and VAL379; and alkyl interactions with ILE155, TYR364, PHE382, and VAL379. Methicillin formed a hydrogen bond with LYS383; vdW interactions with TYR328, GLY330, GLY331, ARG337, SER342, GLN346, GLY365, and ASP376; pi–pi T-shaped interaction with PHE382; pi-alkyl interaction with VAL379; and alkyl interactions with PHE149, TYR327, VAL379, and PHE382. The 1B domain of FemA has been reported as the only active site of the protein. Interestingly, the hit compounds of this study interacted with the residues reported by Rahman and Das as being present in this domain [41].

All the hit compounds were predicted to be drug-like, showcasing their potential to serve as oral drugs. Noteworthy, the Ro5 is a widely utilized guideline in drug discovery to predict the likelihood of a compound possessing good oral bioavailability [29]. It is employed in the initial stages of drug discovery and it stipulates that a compound should possess a molecular weight below 500 Da, have no more than five hydrogen bond donors, have no more than ten hydrogen bond acceptors, and maintain an octanol-water partition coefficient value below 5. The hit compounds of this study did not violate any of these parameters, hence, their potential viability as orally administered therapeutic agents.

Also, all the compounds exhibited high HIA potential compared to methicillin. Conversely, the Caco-2 permeability potential was high for compounds "135964525" and "44130718," moderate for "135520508" and "methicillin," but very poor for "135438537" and "135505656." The discrepancies observed between the predictions of HIA and Caco-2 permeability can be attributed to several underlying factors. A primary contributor to these divergent outcomes is the differences between the cellular models employed. While Caco-2 cells, derived from human colon carcinoma, are widely utilized as an *in vitro* model to approximate intestinal absorption, they fail to fully model the diverse conditions and cell types present within the human intestinal environment [42]. Moreover, certain compounds may undergo efficient absorption in the human intestine facilitated by active transport mechanisms that are either absent or not widely expressed in Caco-2 cells. Notably, peptide transporters such as PEPT1 and PEPT2, along with other specific transport proteins, can significantly enhance intestinal absorption, yet their functionality in the Caco-2 cell line may not be efficient [43]. Furthermore, the statistical models employed in these analyses are trained on distinct datasets, contributing to the observed variations in their predictive outcomes [31]. Among the compounds, only "135964525" was predicted to be a non-substrate of the P-gp, while "44130718" and methicillin were the non-inhibitors of P-gp I and II. P-gp, an efflux transporter expressed across various tissues in the body, plays a pivotal role in regulating the cellular uptake and distribution of xenobiotic and potentially harmful compounds [44]. Owing to its function as an efflux pump, a compound's potential to serve as a substrate for P-gp can adversely impact its pharmacokinetic profile and overall therapeutic efficacy. The results of this study show all the hit compounds except "135964525" may require higher dosages to attain the desired therapeutic effects, as their active efflux could result in reduced intracellular drug concentrations. The inhibition of P-gp can result in significant drug-drug interactions by inducing the accumulation of other drugs reliant on P-gp for excretion, potentially leading to toxicity or compromised efficacy [45]. The potential of "44130718" to function as a P-gp inhibitor could lead to toxicity if co-administered with other drugs reliant on P-gp for excretion. As regards the distribution of the hit compounds, the fraction unbound of all the compounds except "44130718" was very low. Drugs can bind to plasma proteins such as albumin and alpha-1-acid glycoprotein, resulting in a reduced pharmacological form [46]. Specifically, the fraction unbound is essential for understanding a drug's pharmacokinetics and pharmacodynamics, as only the unbound drug fraction is available to exert

therapeutic effects. Despite the observed high affinities of "135964525," "135438537," and "135505656," their utilization will be greatly limited due to their predicted fraction unbound values. In terms of drug metabolism, the inhibition of cytochrome P450 (CYP450) enzymes plays a critical role in modulating metabolic processes by lowering the enzymatic reaction rates. This phenomenon can decrease the metabolism of drugs, thereby influencing potential drug interactions that affect treatment efficacy and may elevate the occurrence of adverse effects [47]. All the hit compounds were non-substrate and non-inhibitors of CYP2D6 and non-inhibitors of CYP1A2 and CYP2C19, except for "135505656" which can potentially inhibit CYP1A2. As regards excretion, OCT2 plays a significant role in the pharmacokinetics and pharmacodynamics of various drugs by mediating their uptake into renal tubular cells, affecting their excretion and overall disposition. It is predominantly expressed in the basolateral membrane of renal proximal tubules where it facilitates the uptake of endogenous compounds and exogenous substances, including drugs, from the bloodstream into renal cells for subsequent excretion [48]. Drugs that are not substrates for OCT2 may have a longer systemic circulation time and slower renal elimination. This can be beneficial for drugs requiring sustained therapeutic levels or for drugs with a narrow therapeutic index [49]. The inability of all the hit compounds to serve as substrates of OCT2 will potentially constitute an advantage for the compounds due to their low fraction unbound, therefore, helping them achieve prolonged therapeutic effect. Disappointingly, three of the hit compounds exhibited bad safety profiles as they possess the potential to cause mutagenesis, and may cause carcinogenesis [50].

As evident in Figure 3a, the FemA_Apo complex exhibited the least deviation compared to that of the control and the final hits, with an average RMSD of 0.325 ± 2.041 Å. Conversely, the FemA_methicillin complex exhibited an average RMSD of 0.695 ± 3.008 Å, while that of the FemA_135964525 complex was 0.508 ± 1.553 Å. The PBP-2a_Apo complex also recorded minimal RMSD fluctuations compared to the control, with an average RMSD of 0.805 ± 1.072 Å (Figure 3b). The 5M18_44130718 complex maintained a uniform RMSD level and demonstrated the most stable behavior among the complexes. Notably, the PBP-2a_Methicillin (control) complex initially exhibited similar RMSD levels to the 5M18_44130718 complex; however, significant structural deviations were observed between 150 and 200 ns. Similarly, the Apo state of the PBP-2a protein showed consistent levels with minimal deviations, demonstrating a stable structural conformation throughout the simulation period.

In the FemA_Apo protein, the regions between residues 50–80 and 280–300 exhibited fluctuation, with the RMSF value of the 50–80th residues increasing from 7 to 14 Å, while the 280–290th residues showed changes in RMSF to 11 Å, which later reduced to less an average of 2 Å for the remaining. The residues at the termini region of the hit complexes exhibited the highest flexibility, with RMSF value as high as 12.5 Å for FemA_135964525 complex as opposed to the 8 Å for FemA_135964525. The fluctuation of the residues was relatively stable except for the amino acid residues between 220 and 270 which had a high fluctuation. Conversely, the PBP-2a_Methicillin complex residues had higher fluctuation compared to the PBP-2a_44130718 residues. The complexes' residues between 1 and 380 had similar fluctuation profiles, however, the PBP-2a_Methicillin residues at 380 residues and above had a highly unstable fluctuation compared to the hit compound's complexes. These RMSF profiles serve as indicators of structural differences between the control complexes and their respective counterparts, with lower values suggesting greater structural similarity and higher values indicating increased structural divergence.

As evident in Figure 5(a) and (b), all the complexes strongly align with the RMSD results and demonstrated similar levels of Rg, thus showing the same level of protein size during the simulation. The first peak in our Radius of Gyration analysis corresponds to the control complex FemA_methicillin. The calculated Rg value for this complex, 27.3 Å, indicates its compactness and overall structural stability. A lower Rg value for this peak suggests that the control complex maintains a well-folded and comparatively compact conformation. This structural stability is crucial for the normal functioning of the complex. Moving to the second peak, which represents the FemA_135964525, the Rg value of 36.4 Å provides insights into its size and shape compared to the control. A detailed analysis of this peak suggests that FemA_135964525 may exhibit structural differences when compared to the control, potentially indicating a change in its conformational flexibility or compactness. These results are strongly in tandem with the RMSD results thus maintaining a similar level with no significant deviation. This further demonstrates minimal or no unbinding events experienced by the ligand during the simulation.

In the interaction of small molecules with biological targets, the importance of hydrogen bonds cannot be overlooked, due to the role it plays in determining the affinity and specificity of the compounds. Hence, the stability of the hydrogen bonds formed between the complexes was investigated over the 250 ns simulation period. As evident in Figure 6, the average hydrogen bonds in FemA_135964525, and PBP-2a_44130718 complexes remained higher than the control drug. For instance, the PBP-2a_44130718 exhibited the highest number of hydrogen bonds, with about 7 hydrogen bonds between the ligand and receptor during the simulations. The results shown in Figure 7, demonstrate that our identified

hits may strongly inhibit the function of the proteins than the control drug.

The energy decomposition analysis graph describes the total interaction of each residue in drug to binding free with respect target protein. These results reveal important insights into how peptide-drug interactions. Per-residue energy decomposition analysis was conducted on the 250 ns simulation trajectory, revealing the individual residue contributions to the total energy for each system, as illustrated in Figure 7. As evident in Figure 7, it is evident that Tyr327, Ser149, Arg139, Gln292, and Gln292 significantly contributed to the total energy while the other residues such as Phe363, Lys383, Lys148, Glu150, Thr165, Arg24, Val256, Gly271, Lys289 and also contributed to the total energy.

The MMPBSA analysis reveals significant insights into the binding interactions of various drug-protein complexes. For the 1LRZ_methicillin complex, the total binding free energy ($\Delta_{G,Total}$) is −35.41 ± 35.11 kJ/mol, with considerable contributions from vdW (Δ_{vdW}) and electrostatic (Δ_{elec}) interactions. In contrast, the 1LRZ_135964525 complex exhibits a more favorable binding affinity ($\Delta_{G,Total}$ = −42.54 ± 12.30 kJ/mol) due to higher vdW and electrostatic contributions, despite a higher polar solvation energy (Δ_{ps}). Similarly, the 5M18_Methicillin complex shows a $\Delta_{G,total}$ of −31.01 ± 12.21 kJ/mol, indicating slightly less favorable binding compared to the 1LRZ_methicillin complex, but still driven by strong vdW and electrostatic forces.

The 5M18_44130718 complex, with a $\Delta_{G,total}$ of −35.41 ± 11.20 kJ/mol, demonstrates substantial vdW and electrostatic contributions, comparable to the 1LRZ_135964525 complex. These results underscore the critical role of vdW and electrostatic interactions in stabilizing the drug-protein complexes, while variations in polar solvation energy highlight the importance of solvation effects in modulating binding affinities. Overall, the analysis suggests that ligands 135964525 and 44130718 have stronger binding affinities compared to methicillin, offering valuable insights for optimizing drug candidates.

5 Conclusion

In conclusion, this study highlights the potential of two compounds as treatment for MRSA by targeting two key proteins, PBP-2a and FemA. The semi-flexible docking methodology demonstrated that the hit compounds exhibited high affinity for the targets, with notable interactions at crucial binding sites. Furthermore, the compounds' drug-likeness, high human intestinal absorption potential, and favorable interaction profiles with key residues in PBP-2a and FemA, suggest their viability as complementary therapeutic agents. The MD simulations and energy decomposition analyses provided deeper insights into the stability and binding interactions, reinforcing the potential of these compounds to serve as effective alternatives to traditional antibiotics in the fight against MRSA.

Acknowledgements: The authors extend their appreciation to the Researchers Supporting Project number (RSP2024R437), King Saud University, Riyadh, Saudi Arabia.

Funding information: This work is supported by the Researchers Supporting Project number (RSP2024R437), King Saud University, Riyadh, Saudi Arabia.

Author contributions: Conceptualization, writing the original draft, formal analysis: Mohammed Bourhia, Muhammad Shahab, and Guojun Zheng. Investigations, funding acquisition, resources, and project administration: Mohamed Taibi, Amine Elbouzidi, Musaab Dauelbait. Reviewing and editing, data validation, and data curation and supervision: Ahmad Mohammad Salamatullah and Abdeslam Asehraou.

Conflict of interest: The authors declared no potential conflicts of interest with respect to the research, authorship, and/or publication of this article.

Ethical approval: The conducted research is not related to either human or animals use.

Data availability statement: Data will be available upon request from the corresponding author.

References

[1] Doron S, Gorbach SL. Bacterial infections: Overview. In International encyclopedia of public health. Oxford: Elsevier; 2008. p. 273–82. doi: 10.1016/B978-012373960-5.00596-7.

[2] Guo Y, Song G, Sun M, Wang J, Wang Y. Prevalence and Therapies of Antibiotic-Resistance in Staphylococcus aureus. Front Cell Infect Microbiol. Mar. 2020;10:107. doi: 10.3389/fcimb.2020.00107.

[3] Knox J, Uhlemann A-C, Lowy FD. Staphylococcus aureus infections: transmission within households and the community. Trends Microbiol. Jul. 2015;23(7):437–44. doi: 10.1016/j.tim.2015.03.007.

[4] Solberg CO. Spread of Staphylococcus aureus in hospitals: causes and prevention. Scand J Infect Dis. 2000;32(6):587–95. doi: 10.1080/003655400459478.

[5] Creech CB, Al-Zubeidi DN, Fritz SA. Prevention of recurrent staphylococcal skin infections. Infect Dis Clin North Am. Sep. 2015;29(3):429–64. doi: 10.1016/j.idc.2015.05.007.

[6] Rasmussen RV, Fowler VG, Skov R, Bruun NE. Future challenges and treatment of Staphylococcus aureus bacteremia with emphasis on

MRSA. Future Microbiol. Jan. 2011;6(1):43–56. doi: 10.2217/fmb.10.155.

[7] Ye C, Wang C, Li Z, Li X, Pan J, Liu L, et al. The effect of combination therapy on mortality and adverse events in patients with staphylococcus aureus bacteraemia: a systematic review and meta-analysis of randomized controlled trials. Infect Dis Ther. Dec. 2021;10(4):2643–60. doi: 10.1007/s40121-021-00539-y.

[8] Shalaby M-AW, Dokla EME, Serya RAT, Abouzid KAM. Penicillin binding protein 2a: An overview and a medicinal chemistry perspective. Eur J Med Chem. Aug. 2020;199:112312. doi: 10.1016/j.ejmech.2020.112312.

[9] Bush K, Bradford PA. β-Lactams and β-Lactamase inhibitors: An overview. Cold Spring Harb Perspect Med. Aug. 2016;6(8):a025247. doi: 10.1101/cshperspect.a025247.

[10] Otero LH, Rojas-Altuve A, Llarrull LI, Carrasco-López C, Kumarasiri M, Lastochkin E, et al. How allosteric control of *Staphylococcus aureus* penicillin binding protein 2a enables methicillin resistance and physiological function. Proc Natl Acad Sci USA. Oct. 2013;110(42):16808–13. doi: 10.1073/pnas.1300118110.

[11] Li X, Xiong Y, Fan X, Feng P, Tang H, Zhou T. The role of femA regulating gene on methicillin-resistant Staphylococcus aureus clinical isolates. Méd et Mal Infect. May 2012;42(5):218–25. doi: 10.1016/j.medmal.2008.09.031.

[12] Maidhof H, Reinicke B, Blümel P, Berger-Bächi B, Labischinski H. femA, which encodes a factor essential for expression of methicillin resistance, affects glycine content of peptidoglycan in methicillin-resistant and methicillin-susceptible Staphylococcus aureus strains. J Bacteriol. Jun. 1991;173(11):3507–13. doi: 10.1128/jb.173.11.3507-3513.1991.

[13] Ahmed NS, AlFooty KO, Khalifah SS. Synthesis of 1,8-naphthyridine derivatives under ultrasound irradiation and cytotoxic activity against HepG2 cell lines. J Chem. 2014;2014:1–8. doi: 10.1155/2014/126323.

[14] Chukwuemeka PO, Umar HI, Iwaloye O, Oretade OM, Olowosoke CB, Elabiyi MO, et al. Targeting p53-MDM2 interactions to identify small molecule inhibitors for cancer therapy: beyond 'Failure to rescue. J Biomol Struct Dyn. 2021;40:9158–76. doi: 10.1080/07391102.2021.1924267.

[15] Olukunle OF, Olowosoke CB, Khalid A, Oke GA, Omoboyede V, Umar HI, et al. Identification of a 1, 8-naphthyridine-containing compound endowed with the inhibition of p53-MDM2/X interaction signaling: a computational perspective. Mol Divers. Apr. 2023;28:1109–27. doi: 10.1007/s11030-023-10637-3.

[16] Abdul Razak NS, Jamalis J, Chander S, Wahab RA, Bhagwat DP, Smith TK, et al. Coumarin-oxadiazole derivatives: synthesis and pharmacological properties. MROC. Oct. 2020;17(7):780–94. doi: 10.2174/1570193X16666191029111051.

[17] Wang J-J, Sun W, Jia W-D, Bian M, Yu L-J. Research progress on the synthesis and pharmacology of 1,3,4-oxadiazole and 1,2,4-oxadiazole derivatives: a mini review. J Enzyme Inhib Med Chem. Dec. 2022;37(1):2304–19. doi: 10.1080/14756366.2022.2115036.

[18] Usha T, Shanmugarajan D, Goyal AK, Kumar CS, Middha SK. Recent Updates on computer-aided drug discovery: time for a paradigm shift. CTMC. Feb. 2018;17(30):3296–307. doi: 10.2174/1568026618666180101163651.

[19] Bourhia M, Shahab M, Zheng G, Bin Jardan YA, Sitotaw B, Ouahmane L, et al. Napthyridine-derived compounds as promising inhibitors for staphylococcus aureus crtm: a primer for the discovery of potential anti-staphylococcus aureus agents. Front Microbiol. 2023;14:1279082.

[20] Kim S, Chen J, Cheng T, Gindulyte A, He J, He S, et al. PubChem 2019 update: improved access to chemical data. Nucleic Acids Res. Jan. 2019;47(D1):D1102–09. doi: 10.1093/nar/gky1033.

[21] Artemova S, Jaillet L, Redon S. Automatic molecular structure perception for the universal force field. J Comput Chem. May 2016;37(13):1191–205. doi: 10.1002/jcc.24309.

[22] Berman HM. The protein data bank. Nucleic Acids Res. Jan. 2000;28(1):235–42. doi: 10.1093/nar/28.1.235.

[23] Mahasenan KV, Molina R, Bouley R, Batuecas MT, Fisher JF, Hermoso JA, et al. Conformational dynamics in penicillin-binding protein 2a of methicillin-resistant *staphylococcus aureus*, allosteric communication network and enablement of catalysis. J Am Chem Soc. Feb. 2017;139(5):2102–10. doi: 10.1021/jacs.6b12565.

[24] Benson TE, Prince DB, Mutchler VT, Curry KA, Ho AM, Sarver RW, et al. X-Ray crystal structure of staphylococcus aureus FemA. Structure. Aug. 2002;10(8):1107–15. doi: 10.1016/S0969-2126(02)00807-9.

[25] Pettersen EF, Goddard TD, Huang CC, Couch GS, Greenblatt DM, Meng EC, et al. UCSF Chimera? A visualization system for exploratory research and analysis. J Comput Chem. Oct. 2004;25(13):1605–12. doi: 10.1002/jcc.20084.

[26] Guex N, Peitsch MC. SWISS-MODEL and the Swiss-Pdb Viewer: An environment for comparative protein modeling. Electrophoresis. 1997;18(15):2714–23. doi: 10.1002/elps.1150181505.

[27] Trott O, Olson AJ. AutoDock Vina: Improving the speed and accuracy of docking with a new scoring function, efficient optimization, and multithreading. J Comput Chem. 2009;31:455–61. doi: 10.1002/jcc.21334.

[28] Biovia DS. Discovery studio modeling environment, release 2017. San Diego: Dassault Systèmes; 2016. Available from: (Accessed 1 September 2016).

[29] Lipinski CA, Lombardo F, Dominy BW, Feeney PJ. Experimental and computational approaches to estimate solubility and permeability in drug discovery and development settings. Adv Drug Delivery Rev. 1997;23(1):3–25. 1PII of original article: S0169-409X(96)00423-1. The article was originally published in Advanced Drug Delivery Reviews, 46, 1–3, 3–26, Mar. 2001 doi: 10.1016/S0169-409X(00)00129-0.

[30] Daina A, Michielin O, Zoete V. SwissADME: A free web tool to evaluate pharmacokinetics, drug-likness and medicinal chemistry friendliness of small molecules. Sci Rep. 2017;7:42717. doi: 10.1038/srep42717.

[31] Pires DEV, Blundell TL, Ascher DB. pkCSM: predicting small-molecule pharmacokinetic and toxicity properties using graph-based signatures. J Med Chem. May 2015;58(9):4066–72. doi: 10.1021/acs.jmedchem.5b00104.

[32] Case DA, Darden TA, Cheatham III TE, Simmerling CL, Wang J, Duke RE, et al. AMBER 9. San Francisco: University of California; 2006. p. 45.

[33] Pearlman DA, Case DA, Caldwell JW, Ross WS, Cheatham III TE, DeBolt S, et al. AMBER, a package of computer programs for applying molecular mechanics, normal mode analysis, molecular dynamics and free energy calculations to simulate the structural and energetic properties of molecules. Computer Physics Communications. 1995;91(1–3):1–41.

[34] Wang J, Wang W, Huo S, Lee M, Kollman PA. Solvation model based on weighted solvent accessible surface area. The Journal of Physical Chemistry B. 2001;105(21), 5055–67. BIOVIA, D. S. (2016). Discovery studio modeling environment, release 2017. San Diego: DassaultSystèmes, 2016.

[35] Wang J, Wang W, Kollman A, Case DA. Antechamber, an accessory software package for molecular mechanical calculations. J Am Chem Soc. 2001;222(1):2001.
[36] Roe DR, Cheatham TE. PTRAJ and CPPTRAJ: Software for processing and analysis of molecular dynamics trajectory data. J Chem Theory Comput. Jul. 2013;9(7):3084–95. doi: 10.1021/ct400341p.
[37] Genheden S, Ryde U. The MM/PBSA and MM/GBSA methods to estimate ligand-binding affinities. Expert Opin Drug Discovery. May 2015;10(5):449–61. doi: 10.1517/17460441.2015.1032936.
[38] Mishra SK, Koča J. Assessing the performance of MM/PBSA, MM/GBSA, and QM–MM/GBSA approaches on protein/carbohydrate complexes: effect of implicit solvent models, QM methods, and entropic contributions. J Phys Chem B. Aug. 2018;122(34):8113–21. doi: 10.1021/acs.jpcb.8b03655.
[39] Agarwal R, Smith JC. Speed vs Accuracy: effect on ligand pose accuracy of varying box size and exhaustiveness in autodock vina. Mol Inf. Feb. 2023;42(2):e2200188. doi: 10.1002/minf.202200188.
[40] Aribisala JO, Sabiu S. Cheminformatics identification of phenolics as modulators of penicillin-binding protein 2a of staphylococcus aureus: a structure–activity-relationship-based study. Pharmaceutics. Sep. 2022;14(9):1818. doi: 10.3390/pharmaceutics14091818.
[41] Rahman S, Das AK. Integrated multi-omics, virtual screening and molecular docking analysis of methicillin-resistant staphylococcus aureus usa300 for the identification of potential therapeutic targets: an in-silico approach. Int J Pept Res Ther. Dec. 2021;27(4):2735–55. doi: 10.1007/s10989-021-10287-9.
[42] Lea T. Caco-2 cell line. In: Verhoeckx K, Cotter López-Expósito I, Kleiveland C, Lea T, Mackie A, et al. editors. The impact of food bioactives on health. Cham: Springer International Publishing; 2015. p. 103–11. doi: 10.1007/978-3-319-16104-4_10.
[43] Lopez-Escalera S, Wellejus A. Evaluation of Caco-2 and human intestinal epithelial cells as *in vitro* models of colonic and small intestinal integrity. Biochem Biophys Rep. Sep. 2022;31:101314. doi: 10.1016/j.bbrep.2022.101314.
[44] Ahmed Juvale II, Abdul Hamid AA, Abd Halim KB, Che Has AT. P-glycoprotein: new insights into structure, physiological function, regulation and alterations in disease. Heliyon. Jun. 2022;8(6):e09777. doi: 10.1016/j.heliyon.2022.e09777.
[45] Karthika C, Sureshkumar R. P-Glycoprotein efflux transporters and its resistance its inhibitors and therapeutic aspects. In: Nunes ACF, editor. Biomarkers and bioanalysis overview. IntechOpen; 2021. p. 1–19. doi: 10.5772/intechopen.90430.
[46] Di L. An update on the importance of plasma protein binding in drug discovery and development. Expert Opin Drug Discovery. Dec. 2021;16(12):1453–65. doi: 10.1080/17460441.2021.1961741.
[47] Deodhar M, Al Rihani SB, Arwood MJ, Darakjian L, Dow P, Turgeon J, et al. Mechanisms of CYP450 inhibition: understanding drug-drug interactions due to mechanism-based inhibition in clinical practice. Pharmaceutics. Sep. 2020;12(9):846. doi: 10.3390/pharmaceutics12090846.
[48] Belzer M, Morales M, Jagadish B, Mash EA, Wright SH. Substrate-dependent ligand inhibition of the human organic cation transporter OCT2. J Pharmacol Exp Ther. Aug. 2013;346(2):300–10. doi: 10.1124/jpet.113.203257.
[49] Suo Y, Wright NJ, Guterres H, Fedor JG, Butay KJ, Borgnia MJ, et al. Molecular basis of polyspecific drug and xenobiotic recognition by OCT1 and OCT2. Nat Struct Mol Biol. Jul. 2023;30(7):1001–11. doi: 10.1038/s41594-023-01017-4.
[50] Vijay U, Gupta S, Mathur P, Suravajhala P, Bhatnagar P. Microbial mutagenicity assay: ames test. Bio-Protocol. 2018;8(6):2763. doi: 10.21769/BioProtoc.2763.